Aero-optic imaging deviation prediction based on ISSA-ELM*

XU Liang[1], ZHAO Shiwei[1], and WANG Tao[2]**

1. Tianjin Key Laboratory for Control Theory & Applications in Complicated Systems, School of Electrical Engineering and Automation, Tianjin University of Technology, Tianjin 300384, China

2. School of Intelligent Engineering, Sun Yat-sen University, Guangzhou 510275, China

(Received 4 August 2022; Revised 21 September 2022)

When the aircraft is moving at high speed in the atmosphere, aero-optical imaging deviation will appear due to the influence of aero-optical effect. In order to achieve real-time compensation during the flight of the aircraft, it is necessary to analyze and predict the obtained imaging deviation data. In order to improve the search speed and accuracy of the prediction algorithm and the ability to jump out of local optimum, in this paper, an improved sparrow search algorithm optimized extreme learning machine (ISSA-ELM) neural network model is proposed to predict the aero-optical imagine deviation. Finally, the performance of ISSA-ELM, ELM neural network and SSA-ELM neural network was tested. The results showed that compared with ELM and SSA-ELM algorithms, the convergence speed of ISSA-ELM was significantly enhanced, and the accuracy of data prediction was also significantly improved.

Document code: A **Article ID:** 1673-1905(2023)07-0425-7

DOI https://doi.org/10.1007/s11801-023-2141-y

When the infrared guided aircraft moves at a high speed in the atmosphere, a non-uniform flow field will be generated at the head of the aircraft, and both the beam generation and the beam absorption system will be affected by this flow field, which is called aero-optical effect. Because of aero-optics effect, the light will be deflected when passing through the aero-optics flow field. At this time, the light will have a difference between the imaging position with and without aero-optics flow field, and this imaging deviation is aero-optics imaging deviation[1-5]. Practice has proved that the infrared guided aircraft will be affected by altitude, Mach number, angle of attack and line-of-sight angle during flight. However, in the process of practical application, the system cannot have only one calculation state. In order to achieve real-time compensation of imaging deviation, it is necessary to analyze and predict the obtained imaging deviation data[6]. In order to meet the time of imaging deviation compensation by airborne optical system, intelligent optimization algorithm is used to predict the imaging deviation, which is of great significance to the future military system.

Back propagation (BP) neural network training speed is slow, easy to fall into the local minimum point, extreme learning machine (ELM) neural network improved and optimized BP neural network, randomly generated input layer and hidden layer connection weight and hidden neuron threshold, improve the learning efficiency, and the parameter setting is omitted[7]. When ELM is used to solve the prediction problem, input weight and hidden layer neuron threshold directly determine the accuracy of prediction results, and appropriate input weight and threshold can effectively improve the prediction accuracy. However, the random generation of input weight and hidden layer neuron threshold of ELM is easy to lead to divergence of prediction results. The classical idea is to use swarm intelligence algorithm to optimize and generate input weight and hidden layer neuron threshold of ELM, and to transform the solving of input weight and hidden layer neuron threshold of ELM into an optimal solution problem[8-10]. In this paper, the weight and threshold of ELM are optimized by the improved sparrow search algorithm (ISSA).

The optimization of input weight and neuron threshold of hidden layer by particle swarm optimization (PSO) algorithm will have the problem of slow iterative convergence and easy to fall into local optimal[11], and the performance of a PSO depends on its topology, and there is no optimal topology for all problems[12]. ZHU et al[13] introduced differential evolution into ELM and proposed an evolutionary ELM (E-ELM) algorithm. The algorithm uses simple differential variation and crossover operators, and searches for the optimal input weights and hidden bias according to the dynamic adjustment of the whole population, so as to obtain a

* This work has been supported by the National Natural Science Foundation of China (Nos.61975151 and 61308120).

** E-mail：liangx999@163.com

more compact network structure. However, the control parameters generated in this algorithm need to be set manually, and the operation is complicated and time-consuming. CAO et al[14] proposed an adaptive E-ELM algorithm. The algorithm can adjust the crossover probability and scaling factor adaptively, which improves the convergence of the algorithm, but cannot deal with the problem of data imbalance. QI et al[15] proposed to use genetic algorithm (GA) to optimize ELM to predict solar radiation, which improved the prediction accuracy of ELM, but the optimization effect decreased and the time was long in the case of too much data. Based on this, there are many different types of algorithms available in the existing literature. Each algorithm has its own advantages, but it also has disadvantages. For example, PSO in the above literature is easy to premature convergence. GA's search speed is slow. The sparrow optimization algorithm adopted in this paper overcomes these shortcomings to some extent. The algorithm has fast convergence speed and good stability, and is superior to other algorithms to some extent[16,17]. But SSA, like other population algorithms, is easy to fall into local optimum, and the global search ability is weak, through the improvement of sparrow algorithm, the algorithm can obtain higher prediction accuracy and accuracy, and expand the global search, avoid falling into local optimization.

Aero optical imaging deviation is mainly calculated through wind tunnel experiment or computational fluid dynamics (CFD) software, the imaging deviation data in this paper are obtained through a series of CFD calculations.

During the flight of infrared guided aircraft, there will be different flight conditions, such as the current flight height, flight speed, etc. Many research and tests show that the imaging deviation is mainly affected by the altitude, Mach number, angle of attack and line-of-sight angle. When a certain factor changes, the imaging deviation also changes, that is, the influence of a single factor on the imaging deviation. For example, when the flight altitude of the aircraft increases, the imaging deviation decreases gradually. When the flight speed of the aircraft increases, the imaging deviation increases gradually.

However, a flight condition can only represent the current conditions of four factors, which are independent relations. Therefore, in this paper, the above four factors are used as input variables, and the imaging deviation, is used as output variables.

But CFD this experimental method has high cost and long calculation time. A lot of calculations need to be done for each aircraft. However, because the data obtained in the experiment is not enough, and the working state of airborne optical system is not the only one, there will be many accidents. Therefore, we need to analyze these discrete data and establish a reliable prediction model.

ELM is a single hidden layer feedforward neural network, which can randomly initialize the input weight and bias, obtain the corresponding output weight. Its structure is shown in Fig.1[18].

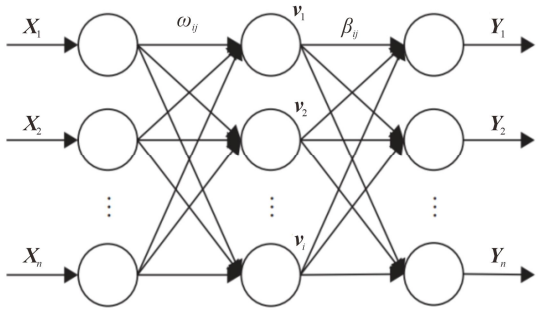

Fig.1 Typical ELM neural network

In the figure above, $\boldsymbol{X}_n$ is the n-dimensional input vector and $\boldsymbol{Y}_m$ is the m-dimensional target vector. Then the output of an ELM neural network with i hidden layers is

$$\boldsymbol{Y}_j = \sum_{i=1}^{n} \beta_i G\left(\omega_i \boldsymbol{X}_j + \boldsymbol{v}_i\right), j = 1,2,\cdots,n, \tag{1}$$

where ω_i is the weight between input layer and hidden layer, β_i is the weight between input layer and hidden layer, $\boldsymbol{v}_i$ is the threshold of the hidden layer neurons, and $G(x)$ is the activation function.

$$\boldsymbol{H}_{\omega,\boldsymbol{v},\boldsymbol{X}}\beta = \boldsymbol{T}, \tag{2}$$

where $\boldsymbol{T}$ is the expected output vector, and $\boldsymbol{H}_{\omega,\boldsymbol{v},\boldsymbol{X}}$ is the output matrix of hidden layer. It can be expressed as

$$\boldsymbol{H}_{\omega,\boldsymbol{v},\boldsymbol{X}} = \begin{bmatrix} G\left(\omega_1 \boldsymbol{X}_1 + \boldsymbol{v}_1\right) & \cdots & G\left(\omega_i \boldsymbol{X}_1 + \boldsymbol{v}_i\right) \\ \vdots & \ddots & \vdots \\ G\left(\omega_1 \boldsymbol{X}_n + \boldsymbol{v}_1\right) & \cdots & G\left(\omega_i \boldsymbol{X}_n + \boldsymbol{v}_i\right) \end{bmatrix}. \tag{3}$$

The output weight β^* can be solved using the following equation:

$$\beta^* = \boldsymbol{H}^+ \boldsymbol{T}, \tag{4}$$

where $\boldsymbol{H}^+$ is the generalized inverse of the Moore-Penrose output matrix $\boldsymbol{H}$ of the hidden layer.

The SSA is inspired by the sparrow's behavior of looking for food and anti-predation in the biological world. Its main rules are as follows. The discoverer in the sparrow is responsible for searching for areas with food and water sources in the whole population, and providing foraging areas and directions for all participants. When the sparrow finds a predator, the vigilant will sound an alarm, and the sparrow at the edge of the group will quickly move to a safe area and get a better position. When the alarm signal is greater than the safe value, the discoverer will lead other sparrows and newly added sparrows to find food in other safe places. The foraging position of the population is related to the energy of the participants. In the process of foraging, participants can always find the best discoverer, follow the discoverer to get food and forage in the area found by the discoverer. Some participants even continuously monitor the discoverer in order to increase their

predation rate[16].

$$\boldsymbol{X}=\left[\boldsymbol{x}_1,\boldsymbol{x}_2\cdots\boldsymbol{x}_n\right]^{\mathrm{T}},\boldsymbol{x}_i=\left[x_{i,1},x_{i,2}\cdots x_{i,d}\right], \tag{5}$$

where n is the number of sparrows, i=1, 2,…, n, d is the dimension of the variable, and the fitness matrix of sparrow is:

$$\boldsymbol{F}_x=\left[f\left(\boldsymbol{x}_1\right),f\left(\boldsymbol{x}_2\right)\cdots f\left(\boldsymbol{x}_n\right)\right]^{\mathrm{T}}, \tag{6}$$

$$f\left(\boldsymbol{x}_i\right)=\left[f\left(x_{i,1}\right),f\left(x_{i,2}\right)\cdots f\left(x_{i,d}\right)\right], \tag{7}$$

where each value in $\boldsymbol{F}_x$ represents the fitness value of an individual.

Sparrows with good adaptability will give priority to the best position, and these sparrows will lead the population to live in a place rich in food and water as discoverers. The location formula of these discoverers is as follows:

$$\boldsymbol{X}_{i,j}^{t+1}=\begin{cases}\boldsymbol{X}_{i,j}^{t}\cdot\exp\left(\dfrac{-i}{\alpha\cdot iter_{\max}}\right) & R_2<ST\\ \boldsymbol{X}_{i,j}^{t}+Q\cdot\boldsymbol{L} & R_2\geqslant ST\end{cases}, \tag{8}$$

where t represents the number of iterations at that time, j=1, 2,…, d, and $\boldsymbol{X}_{i,j}^{t}$ represents the position of the ith sparrow in dimension j. $iter_{\max}$ is the maximum number of iterations, α is a random number ranging from 0 to 1, R_2 ($R_2\in[0, 1]$) represents the warning value, and ST ($ST\in[0.5, 1]$) represents the safe value. Q is a random number with normal distribution from 0 to 1, $\boldsymbol{L}$ is 1 by d multidimensional matrix, and the matrix entries are all 1's. When $R_2<ST$, it means that the finder has no natural enemies in the search area, so they can expand the search area. When $R_2\geq ST$, it means that the warning value is higher than the safety value, so they should fly to the safe area as soon as possible.

Following the discoverers are those who participant, and their positions are determined by

$$\boldsymbol{X}_{i,j}^{t+1}=\begin{cases}Q\cdot\exp\left(\dfrac{\boldsymbol{X}_{\mathrm{worst}}^{t}-\boldsymbol{X}_{i,j}^{t}}{i^2}\right) & i>\dfrac{n}{2}\\ \boldsymbol{X}_{p}^{t+1}+\left|\boldsymbol{X}_{i,j}^{t}-\boldsymbol{X}_{p}^{t+1}\right|\cdot\boldsymbol{A}^{+}\cdot\boldsymbol{L} & \text{other}\end{cases}, \tag{9}$$

where $\boldsymbol{X}_{\mathrm{worst}}$ represents the global worst position, and $\boldsymbol{A}$ is the multidimensional matrix of $1\times d$, but the elements in the matrix are −1 and 1 of random numbers, and $\boldsymbol{A}^{+}=\boldsymbol{A}^{\mathrm{T}}(\boldsymbol{A}\boldsymbol{A}^{\mathrm{T}})^{-1}$. When $i>n/2$, it means that the ith participant with poor fitness value does not get food, the energy value is very low, and needs to go elsewhere to get more food.

Generally, 10%—20% of sparrows in a population will act as the vigilant of the whole population, and its position update formula is

$$\boldsymbol{X}_{i,j}^{t+1}=\begin{cases}\boldsymbol{X}_{\mathrm{best}}^{t}+\beta\cdot\left|\boldsymbol{X}_{i,j}^{t}-\boldsymbol{X}_{\mathrm{best}}^{t}\right| & f_i>f_{\mathrm{g}}\\ \boldsymbol{X}_{i,j}^{t}+k\cdot\left(\dfrac{\left|\boldsymbol{X}_{i,j}^{t}-\boldsymbol{X}_{\mathrm{worst}}^{t}\right|}{\left(f_i-f_{\mathrm{w}}\right)+\varepsilon}\right) & f_i=f_{\mathrm{g}}\end{cases}, \tag{10}$$

where $\boldsymbol{X}_{\mathrm{best}}$ represents the global best position, β is a normal distribution random number with mean value of 0 and variance of 1, and a uniform random number in the range of $k\in[-1, 1]$. f_i is the fitness value of the current sparrow, f_{a} is the global optimal fitness value, and f_{w} is the global worst fitness value. ε is to avoid constants with a denominator of 0 that are not 0 when $f_i>f_{\mathrm{a}}$, indicating that the population is at the edge of danger and threatened by natural enemies, when $f_i=f_{\mathrm{a}}$ indicates that the sparrows in the middle of the population are aware of the attack of natural enemies and need to be close to the safe area. k is the step control parameter.

In the basic SSA, in $R_2<ST$, with the increase of the number of iterations, each dimension of sparrow decreases with the increase of the number of iterations, so the search element space decreases and the probability of falling into local is increased. Sine cosine learning factor is added to improve the ability of global exploration. The improved discoverer location formula is[17,19]

$$\omega=\omega_{\min}+\left(\omega_{\max}-\omega_{\min}\right)\cdot\sin\left(t\pi/iter_{\max}\right), \tag{11}$$

$$\boldsymbol{X}_{i,j}^{t+1}=\begin{cases}(1-\omega)\cdot\boldsymbol{X}_{i,j}^{t}+\omega\cdot\sin\left(r_1\right)\cdot\left|r_2\cdot\boldsymbol{X}_{\mathrm{best}}-X_{i,j}^{t}\right| & R_2<ST\\ (1-\omega)\cdot\boldsymbol{X}_{i,j}^{t}+\omega\cdot\cos\left(r_1\right)\cdot\left|r_2\cdot\boldsymbol{X}_{\mathrm{best}}-X_{i,j}^{t}\right| & R_2\geqslant ST\end{cases}, \tag{12}$$

where r_1 is a random number from 0 to 2π, and r_2 is a random number from 0 to 2.

Lévy flight refers to the probability of step size, which is a random walk with heavy tail distribution. Its advantage is that continuous small steps and occasional large strides occur randomly, which can expand the search range. In this way, we can jump out of the local optimum and achieve the purpose of global search. The improved formula is as follows[19,20]

$$\boldsymbol{X}_{i,j}^{t+1}=\begin{cases}Q\cdot\exp\left(\dfrac{\boldsymbol{X}_{\mathrm{worst}}^{t}-\boldsymbol{X}_{i,j}^{t}}{i^2}\right) & i>\dfrac{n}{2}\\ \boldsymbol{X}_{\mathrm{p}}^{t+1}+\boldsymbol{X}_{\mathrm{p}}^{t+1}\otimes\mathrm{Levy}(d) & \text{other}\end{cases}, \tag{13}$$

where $\boldsymbol{X}_{\mathrm{p}}^{t+1}$ is the best position for the current discoverer, and Lévy formula is

$$\mathrm{Levy}(x)=0.01\times\frac{r_3\times\sigma}{\left|r_4\right|^{(1/\rho)}}, \tag{14}$$

where r_3 and r_4 are random numbers within the range of [0,1], ρ can be taken as 1.5, and σ is calculated as follows

$$\sigma=\left(\frac{\Gamma(1+\xi)\times\sin(\pi\xi/2)}{\Gamma((1+\xi)/2)\times\xi\times2^{((\xi-1)/2)}}\right)^{(1/\xi)}, \tag{15}$$

where

$$\Gamma(x)=(x-1)!. \tag{16}$$

In the following, PSO, GA, basic SSA and ISSA are selected to compare the selected basic functions for performance test results, and the common parameters of the four algorithms PSO, GA, SSA and ISSA are uniformly set[21].

Tab.1 Test function

Function expression	Data range	Optimum solution
F1	[-100, 100]	0
F3	[-100, 100]	0
F7	[-1.28, 1.28]	0

In the above table, formula F1, F3 and F7 are

$$f_1(x)=\sum_{i=1}^{n}x_i^2, \tag{17}$$

$$f_3(x)=\sum_{i=1}^{n}\left(\sum_{j-1}^{i}x_j\right)^2, \tag{18}$$

$$f_7(x)=\sum_{i=1}^{n}ix_i^4+\text{random}[0,1). \tag{19}$$

It can be seen from Figs.2—4 and Tab.2 that both SSA and ISSA find the optimal value in F1 and F3 test functions, while GA and PSO algorithm do not find the optimal value. Although both SSA and ISSA find the optimal value, the worst value and average value of ISSA are much better than SSA. In the F5 test function, although the optimal value of the four functions is not found, ISSA can obviously find the optimal value faster than the other three algorithms, and the optimal value of ISSA is the closest to the theoretical optimal value. Among all the test functions selected, ISSA has the lowest average value and the worst value compared with the other three algorithms, indicating that ISSA has the highest accuracy and the best stability.

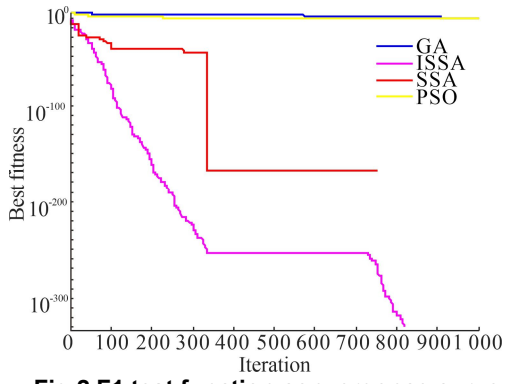

Fig.2 F1 test function convergence curve

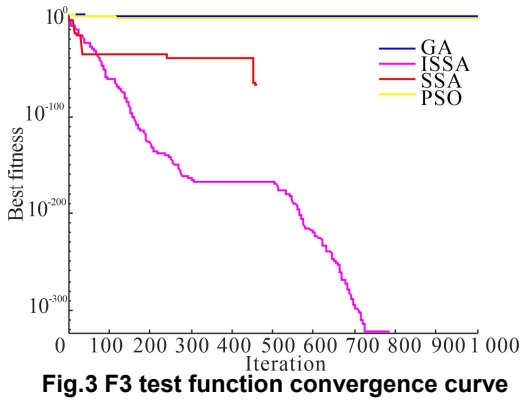

Fig.3 F3 test function convergence curve

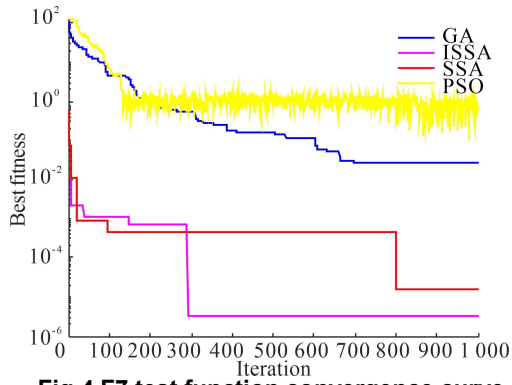

Fig.4 F7 test function convergence curve

Tab.2 Test function result

Test function	Algorithm	Average value	Optimum value	Worst value
F1	PSO	0.386 33	0.216 61	0.599 17
	GA	1.696	0.668 99	7.602 5
	SSA	$7.190\ 7\times10^{-45}$	0	$2.157\ 2\times10^{-43}$
	ISSA	$1.554\ 8\times10^{-131}$	0	$4.664\ 3\times10^{-130}$
F3	PSO	23.627 2	7.567 1	34.507 2
	GA	20.199 4	10.627 1	39.742 9
	SSA	$3.439\ 7\times10^{-51}$	0	$1.031\ 9\times10^{-49}$
	ISSA	$1.151\ 9\times10^{-117}$	0	$3.455\ 8\times10^{-116}$
F7	PSO	1.575 6	0.437 45	9.201 9
	GA	0.043 882	0.026 566	0.087 184
	SSA	0.000 294 87	$1.615\ 7\times10^{-5}$	0.001 107 5
	ISSA	$8.281\ 3\times10^{-5}$	$3.380\ 6\times10^{-6}$	0.000 366 65

The specific flow of ISSA-ELM algorithm is as follows[20,21].

(1) Determine the topology of ELM algorithm.

(2) The migration data of pneumatic imaging were analyzed and processed.

(3) Initialize the SSA.

(4) The fitness of each individual sparrow was calculated.

(5) Update the position formula of sparrow finders and followers according to Eqs.(11—16).

(6) Update the fitness and judge whether the maximum number of iterations or the set convergence accuracy is reached. If so, proceed to the next step; otherwise, return to (4).

(7) The obtained group optimal individual value is assigned to the weight and threshold value in the ELM neural network.

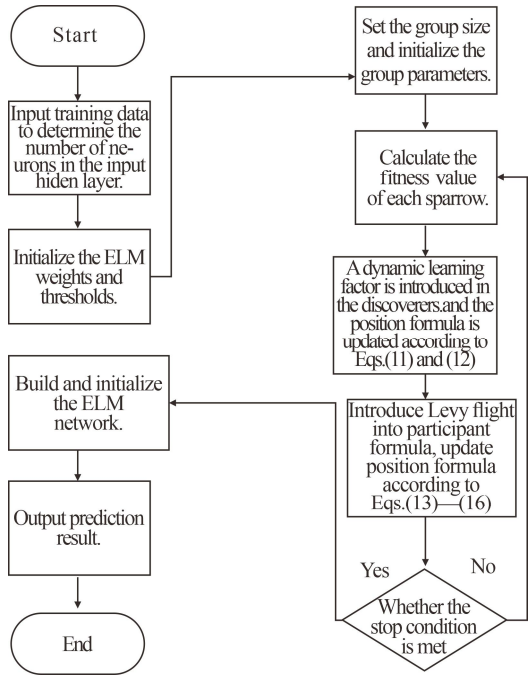

Fig.5 Flow chart based on ISSA-ELM algorithm

ISSA-ELM uses ISSA to optimize the weight and threshold of ELM algorithm, so the four main factors affecting the imaging deviation are taken as the input of ELM algorithm. The prediction accuracies of ELM, SSA-ELM, and ISSA-ELM are compared. It provides a theoretical basis for the application of ISSA-ELM in aero-optical imaging migration prediction.

In the experiment, 3 317 sets of data in the calculation of aircraft imaging deviation were selected. After normalization of the data, 3 217 data were randomly selected as the model training sample set, and the remaining data were used as the model testing sample set.

The advantages and disadvantages of the algorithm are evaluated by the mean absolute error (*MAE*), mean square error (*MSE*), determination coefficient and fitness between the prediction results of the test set and the real value. *MSE* is defined as[22]

$$MSE=\frac{1}{l}\sum_{i=1}^{l}(\hat{y}_i-y_i)^2. \tag{20}$$

Determination coefficient is

$$R^2=\frac{\left(l\sum_{i=1}^{l}\hat{y}_i y_i-\sum_{i=1}^{l}\hat{y}_i\sum_{i=1}^{l}y_i\right)^2}{\left(l\sum_{i=1}^{l}\hat{y}_i^2-\left(\sum_{i=1}^{l}\hat{y}_i\right)^2\right)\left(l\sum_{i=1}^{l}y_i^2-\left(\sum_{i=1}^{l}y_i\right)^2\right)}. \tag{21}$$

MAE is defined as

$$MAE=\frac{1}{l}\sum_{i=1}^{l}\left|\hat{y}_i-y_i\right|, \tag{22}$$

where l is the total number of test samples, $\hat{y}_i$ is the predicted value of the model, and y_i is the actual value.

The fitness curves of SSA-ELM and ISSA-ELM are shown in the following figures.

By comparing SSA-ELM and ISSA-ELM, it can be found that the convergence speed of ISSA-ELM is nearly twice as fast, which shows that ISSA-ELM has fast iteration times and can quickly find the optimal value.

Figs.8—10 show the absolute error prediction results of different models.

The following is the comparison diagram of the real value and predicted value of the three models (Figs.11—13).

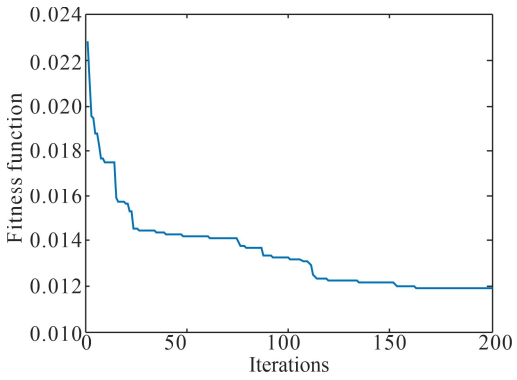

Fig.6 Change diagram of SSA-ELM fitness curve

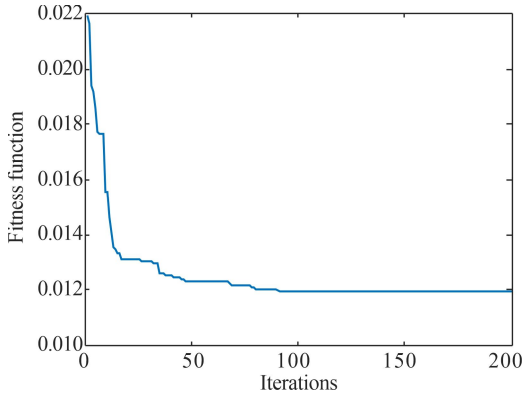

Fig.7 Change diagram of ISSA-ELM fitness curve

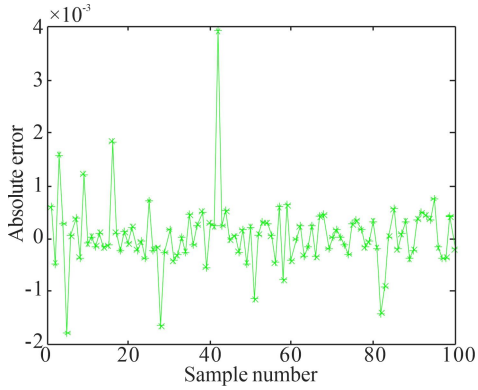

Fig.8 ELM prediction output absolute error

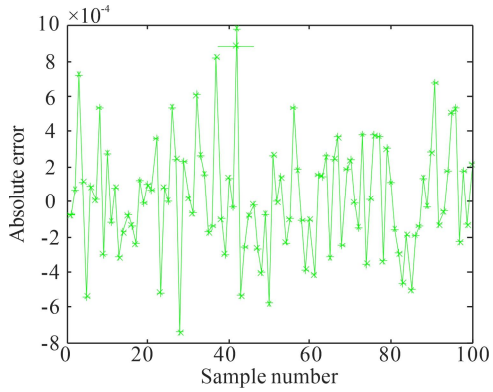

Fig.9 SSA-ELM prediction output absolute error

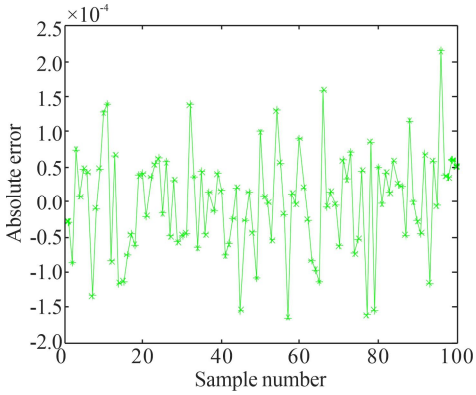

Fig.10 ISSA-ELM prediction output absolute error

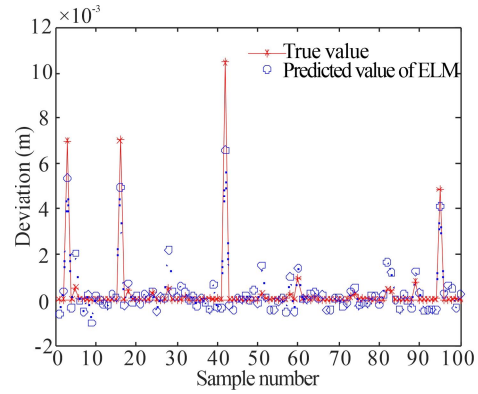

Fig.11 ELM test set prediction results

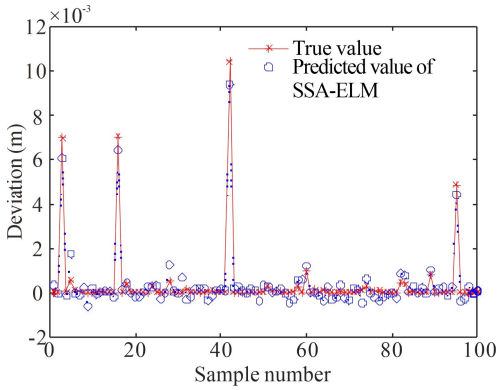

Fig.12 SSA-ELM test set prediction results

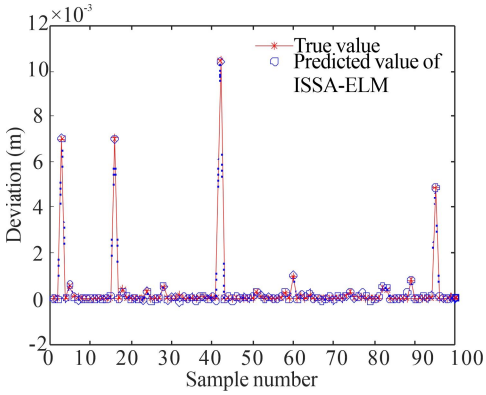

Fig.13 ISSA-ELM test set prediction results

Tab.3 Comparison of prediction results of various models

Model	*MSE*	R^2	*MAE*
ELM	4.138×10^{-7}	0.830 92	0.003 924 0
SSA-ELM	$1.046\ 3\times10^{-7}$	0.955 85	0.000 985 5
ISSA-ELM	$4.664\ 7\times10^{-9}$	0.997 90	0.000 214 6

Figs.8—10 are the absolute error comparison diagrams of ELM, SSA-ELM and ISSA-ELM models, respectively, and Figs.11—13 are the results comparison diagrams of the real value and predicted value of ELM, SSA-ELM and ISSA-ELM models, respectively. Through the analysis and comparison of each model, we can know the following.

In the algorithm model, the *MAE* can accurately reflect the size of the actual prediction error, that is, the smaller the *MAE* is, the higher the prediction accuracy of the model. It can be seen from Figs.8—10 that compared with ELM and SSA-ELM, the prediction accuracy of the ISSA-ELM model is better.

The *MSE* can evaluate the degree of change of the data. The smaller the *MSE*, the better the accuracy of the prediction model in describing the experimental data. In Figs.11—13, compared with the ELM and SSA-ELM, the ISSA-ELM has the smallest *MSE*, indicating that its accuracy is higher.

The coefficient of determination represents the degree of correlation between the actual value and the predicted value. The closer the correlation coefficient of the algorithm model is to 1, the better the algorithm model is. In Figs.11—13, compared with the ELM and SSA-ELM, the coefficient of determination of ISSA-ELM is the closest to 1, indicating that it can make a more perfect prediction of the target variable.

Imaging deviation is due to the head flow field change caused by aircraft, aircraft flying in the actual process, not only a state of flight. When the flight state changes, head flow field will change, and imaging deviation will also change. We calculate the just some typical imaging deviation data, and the data is not enough in actual flight. Therefore, a reliable model is needed to quickly estimate the unknown data through the known imaging offset data, so that the aircraft can be compensated and corrected during the actual flight.

It can be found that the SSA simply optimized the weights and thresholds in the ELM algorithm, which limited the data optimization in this paper and failed to achieve ideal improvement. This is because SSA, like other population algorithms, has weak global search ability and is easy to fall into local optimum. Therefore, the search space and search ability of the algorithm can be improved by the fusion of sine and cosine, and the random walk characteristic of Levy flight can be used to avoid the algorithm falling into local optimum. Through the benchmark function test, it is proved that ISSA can find the optimal value faster than SSA, and ISSA is used to optimize the weights and thresholds of ELM neural network to improve the accuracy of the algorithm. According to the evaluation index of the algorithm, compared with ELM and SSA-ELM models, the prediction accuracy of the ISSA-ELM model is better, and the global convergence and population diversity are guaranteed. It can predict the aero-optical imaging offset more quickly, accurately and stably.

Ethics declarations

Conflicts of interest

The authors declare no conflict of interest.

References

[1] LI G C. Aerooptics[M]. Beijing： National Defense Industry Press, 2006. (in Chinese)

[2] YING L X. A new branch of modern optics - aerooptics[J]. Engineering science, 2005, 7(12)：1-6.

[3] XU L. Aerodynamic optical effect of infrared guided aircraft[D]. Xi'an Jiaotong University, 2012. (in Chinese)

[4] XU L, CAI Y L. Influence of altitude on aero-optic imaging deviation[J]. Applied optics, 2011, 50(18)：2949-2957.

[5] YAO Y, XUE W, WANG T, et al. Influence of LOS angle on aero-optics imaging deviation[J]. OPTIK - international journal for light and electron optics, 2020, 202(163732)：1-5.

[6] XU L, ZHANG Y Z, CHEN X. Aero-optical imaging deviation prediction based on improved sparrow search algorithm and optimized BP neural network[J]. Photoelectron and laser, 2021, 32(06)：653-658.

[7] WANG Z H. BP neural network and ELM algorithm research[D]. China Jiliang University, 2013. (in Chinese)

[8] JIANG S, YANG X Y, LING X S. Evolutionary extreme learning machine optimized by quantum-behaved particle swarm optimization[J]. Journal of system simulation, 2017, 29(10)：219-230.

[9] WU Y. Improved extreme learning machine based on simulated annealing algorithm[J]. Applications of computer systems, 2020, 29(2)：163-168.

[10] LIU Z Z, DU Y, HAN Y X. Drought prediction based on genetic algorithm optimized extreme learning machine model in Yunnan-Guizhou Plateau[J]. Yangtze river, 2020, 51(8)：17-22.

[11] YIN C S, ZHAO T Z. Design and optimization of planetary gear transmission based on particle swarm optimization algorithm[J]. Journal of Tianjin University of Technology, 2021, 168(5)：23-26. (in Chinese)

[12] XU Y, SHU Y. Evolutionary extreme learning machine based on particle swarm optimization[C]//Proceedings of the 3rd International Symposium on Neural Networks, May 28-1 June, 2006, Chengdu, China. Heidelberg：Springer, 2006：644-652.

[13] ZHU Q Y, QIN A K, SUGANTHAN P N. Evolutionary extreme learning machine[J]. Pattern recognition, 2005, 38(10)：1759-1763.

[14] CAO J, LIN Z, HUANG G B. Self-adaptive evolutionary extreme learning machine[J]. Neural processing letters, 2012, 36(3)：285-305.

[15] QI J, LI P. Kansei image evaluation of teacup based on GA-ELM[C]//2018 3rd International Conference on Mechatronics and Information Technology (ICMIT2018), October 30, 2018, Chengdu, China. Beijing：CSP, 2018：1-8.

[16] XUE J K. Research and application of a new type of swarm intelligence optimization technology[D]. Shanghai：Donghua University, 2020. (in Chinese)

[17] LI A L, QUAN L X, CUI G M. Sparrow search algorithm combining sines and cosines with Cauchy variation[J]. Computer engineering and applications, 2022, 58(03)：91-99.

[18] XU R, LIANG X, QI J S, et al. Frontier progress and trends of extreme learning machines[J]. Chinese journal of computers, 2019, 42(07)：1640-1670. (in Chinese)

[19] ZHENG H Q, FENG W J, ZHOU Y Q. Butterfly optimization algorithm based on sine and cosine algorithm[J]. Guangxi science, 2021, 28(02)：152-159.

[20] MA W, ZHU X. Sparrow search algorithm based on Levy flight disturbance strategy[J]. Chinese journal of applied science, 2022, 40(01)：116-130.

[21] XU L, ZHANG Z Y, CHEN X, et al. Aero-optical imaging deviation prediction based on improved sparrow search algorithm and optimized BP neural network[J]. Journal of optoelectronics·laser, 2021, 32(06)：653-658. (in Chinese)

[22] CHEN X. Aero-optics imaging deviation and prediction with different line-of-sight roll angles[D]. Tianjin University of Technology, 2021. (in Chinese)